Chapter 5

Flexure Loading: Experimental Results and Discussion

5.1 Introduction

The experimental results of the out-of-plan bending test are presented in this chapter. Comparisons between the results of test specimens with various types of shear connectors are conducted in this research. The effect of each of type of shear connector was studied on the structural responses in terms of failure load and mode of failure.

5.2 Behaviour Under Flexure Loading

The test set consists of five wall specimens made of AAC blocks and ferrocement sandwich with various types of shear connectors tested for out of plane bending under three line loads. Load, deformation, and strains were recorded using load cell, LVDTs, and strain gauges reader respectively. A dial gauge LVDT was placed under the specimen at the center to measure the deflection versus load. An electrical strain gauge was fixed on each face in order to measure the strain on both faces.

The results of all specimens are listed in Table 5.1. The table shows the ultimate load and the deflection at the ultimate load for each individual specimen and the average ultimate load of each specimen. Figures 5.1 – 5.5 show the load-strain relationships for all specimens.

Table 5.1: Experimental results of the out-of-plane bending test.

Specimen No.	Designation	Type of shear connectors	Deflection at ultimate load (mm)	Ultimate load (kN)	Average ultimate load (kN)
B1	150-FC-Nails	Nails	-	18.80	18.80
B2	150-FC-Cross	Steel cross bracing	0.918	13.41	13.06
B3	150-FC-Cross	Steel cross bracing	0.714	12.71	
B4	150-FC-WM	Welded wire mesh	1.02	15.35	15.23
B5	150-FC-WM	Welded wire mesh	0.816	15.11	

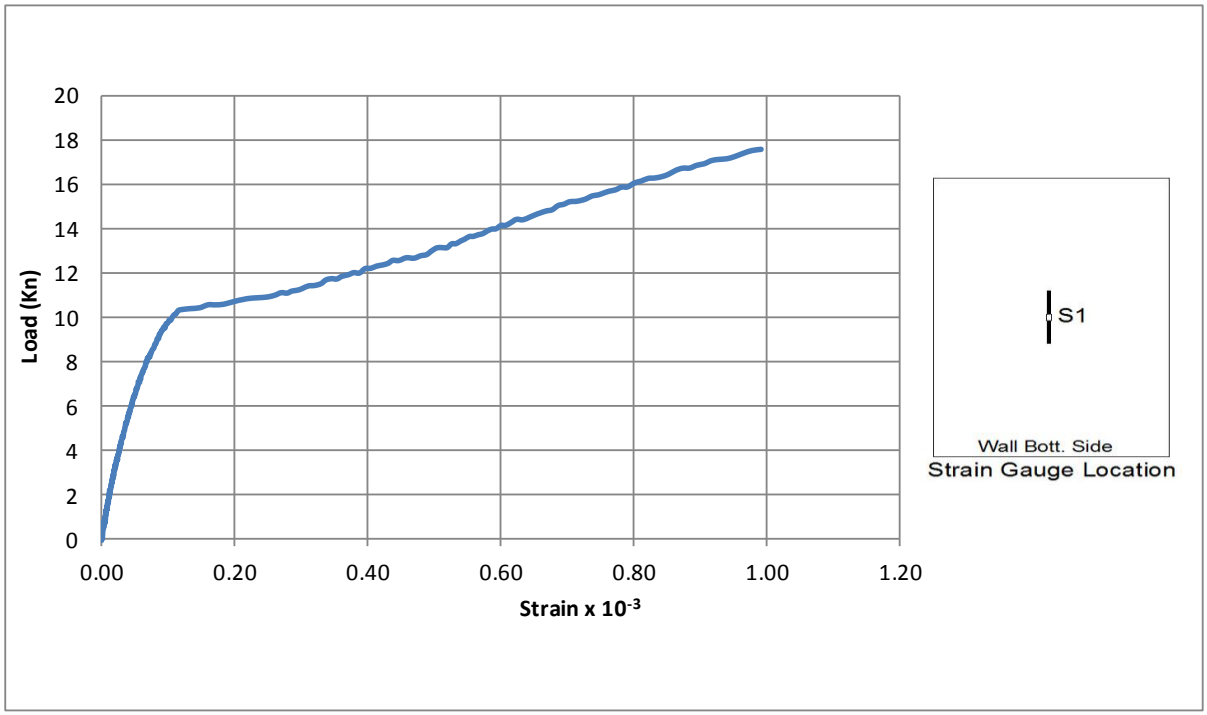

Figure 5.1: Load-strain relationship for Specimen B1 at strain gauge S1

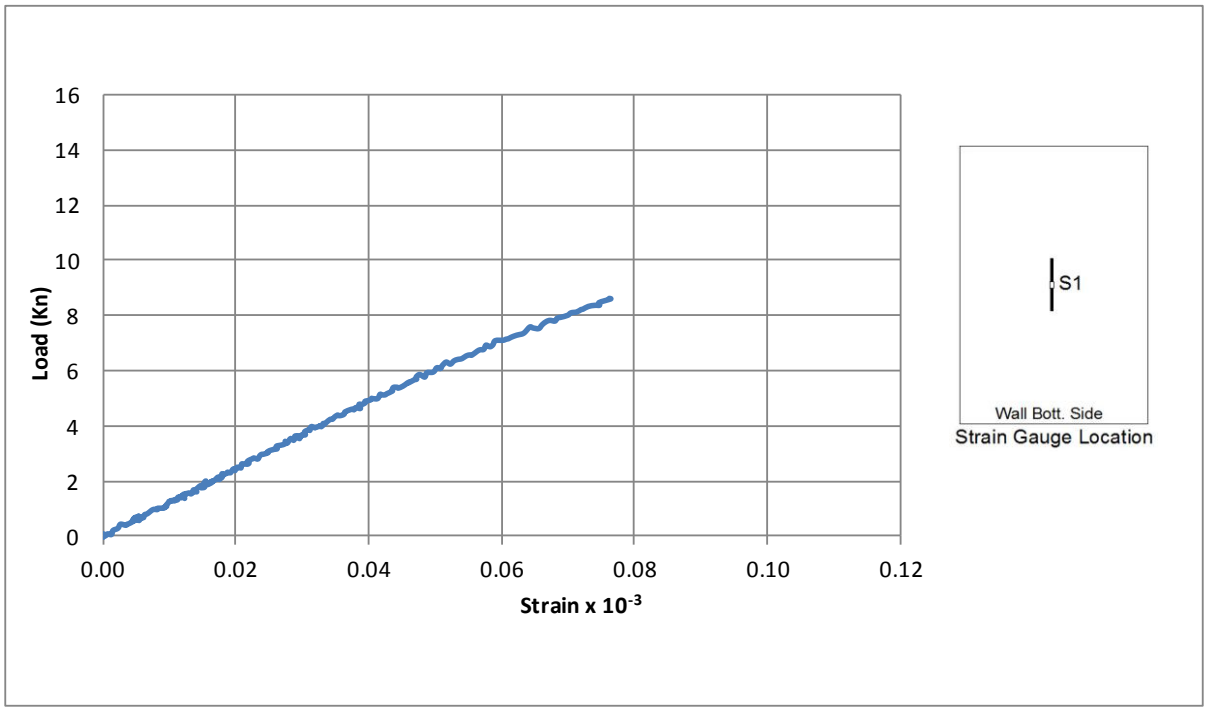

5.2a) Load-strain relationship at strain gauge S1

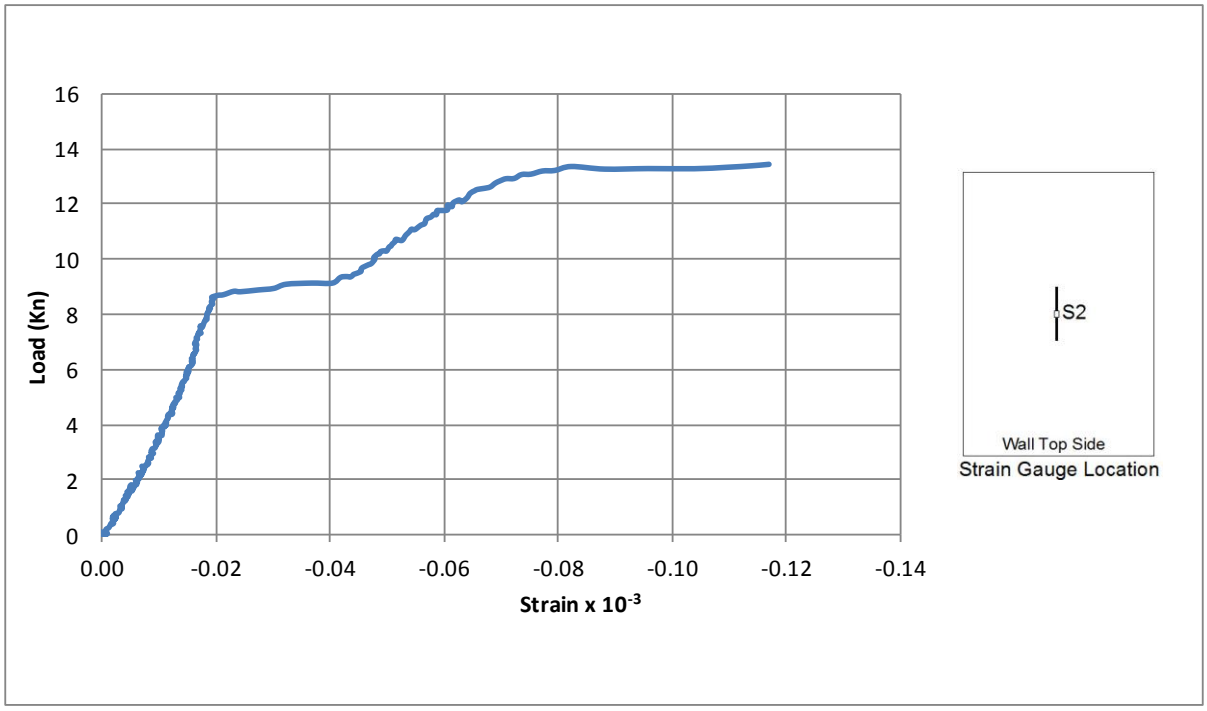

5.2b) Load-strain relationship at strain gauge S2

Figure 5.2: Load-strain relationships for Specimen B2

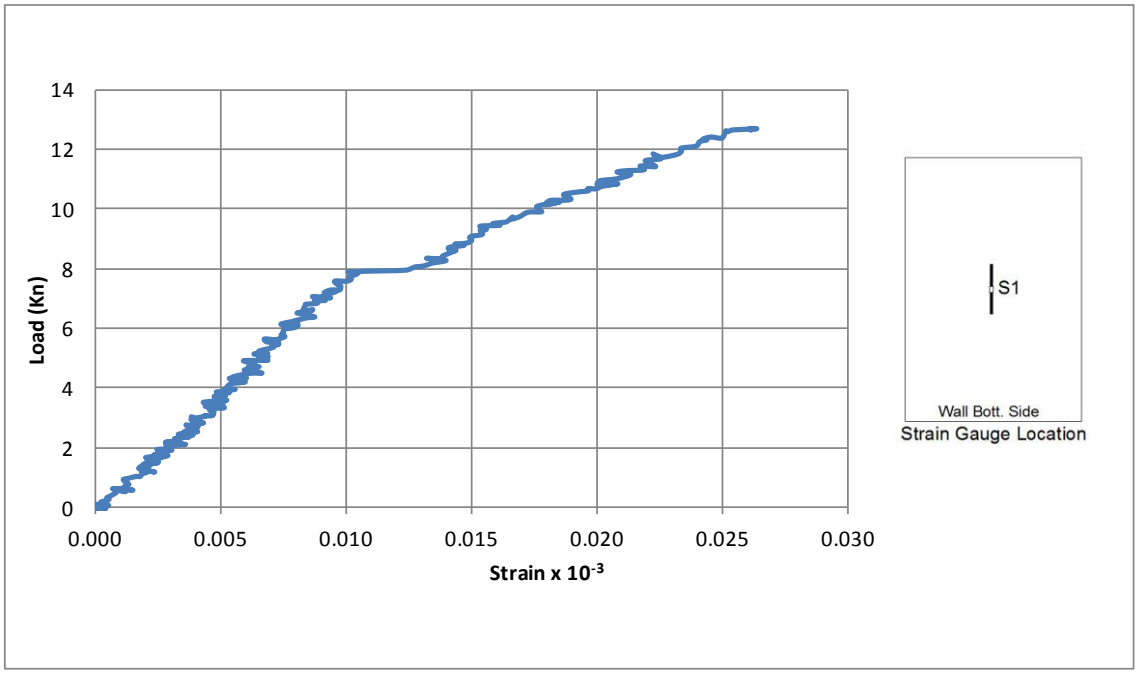

5.3a) Load-strain relationship at strain gauge S1

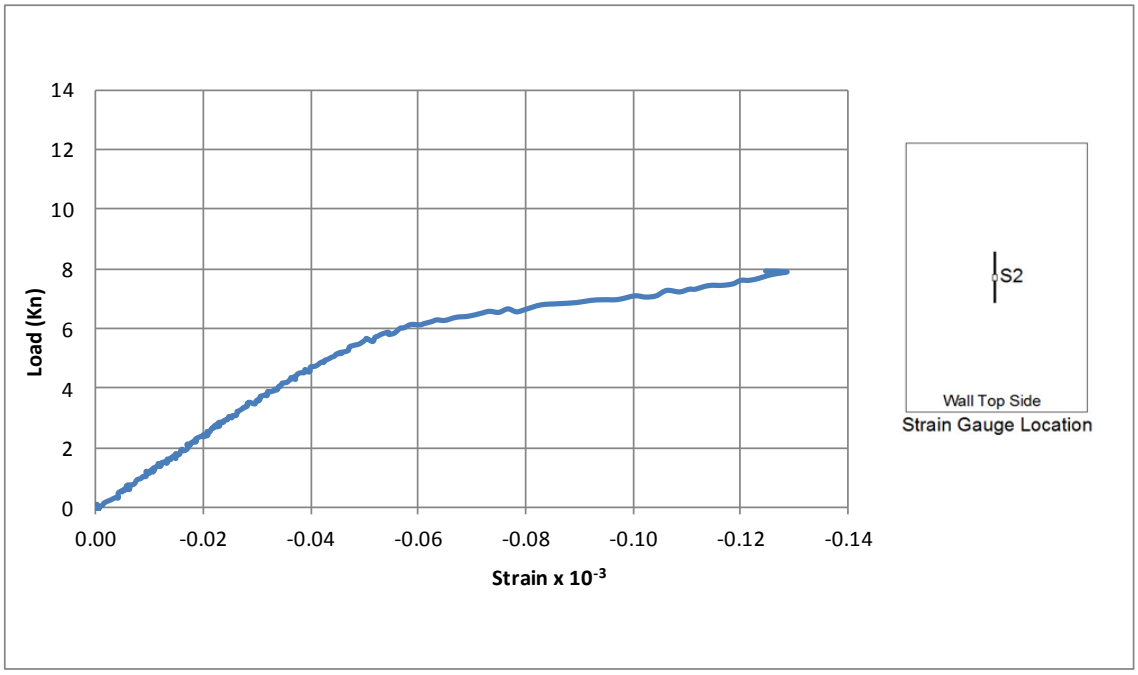

5.3b) Load-strain relationship at strain gauge S2

Figure 5.3: Load-strain relationships for Specimen B3

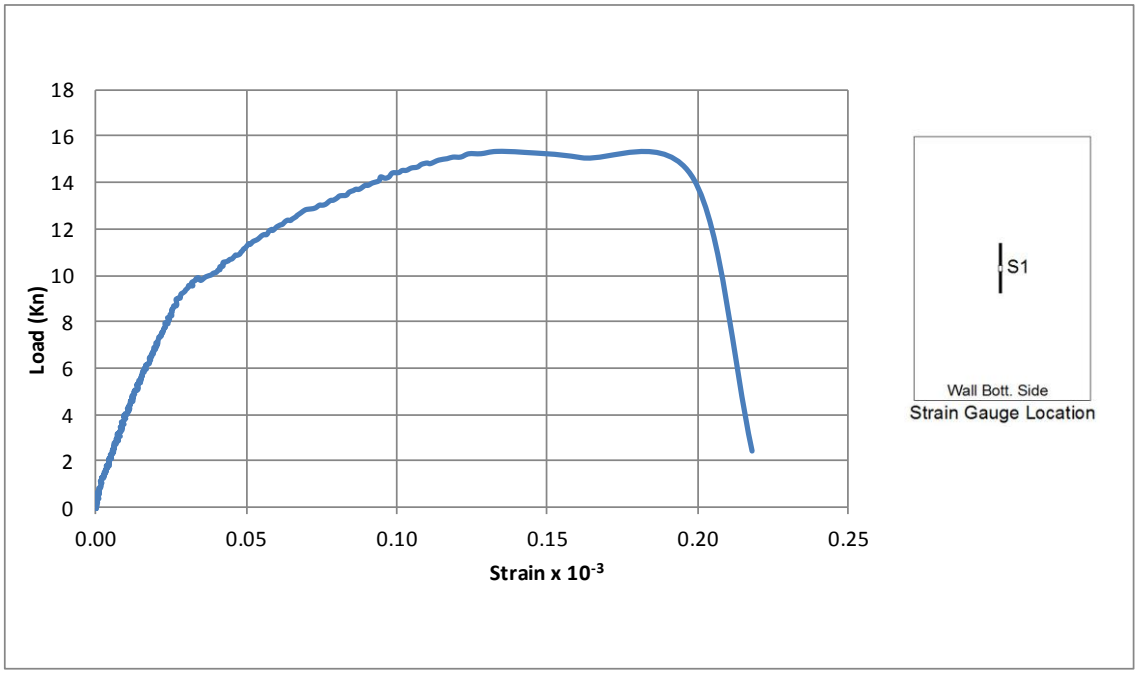

5.4a) Load-strain relationship at strain gauge S1

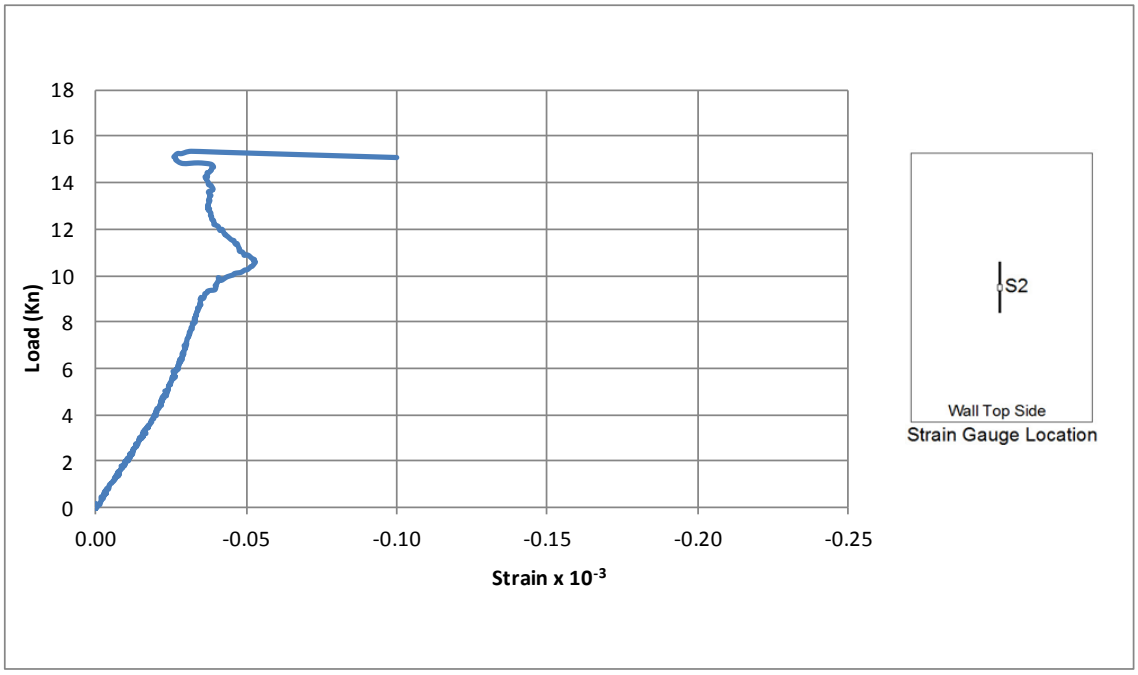

5.4b) Load-strain relationship at strain gauge S2

Figure 5.4: Load-strain relationships for Specimen B4

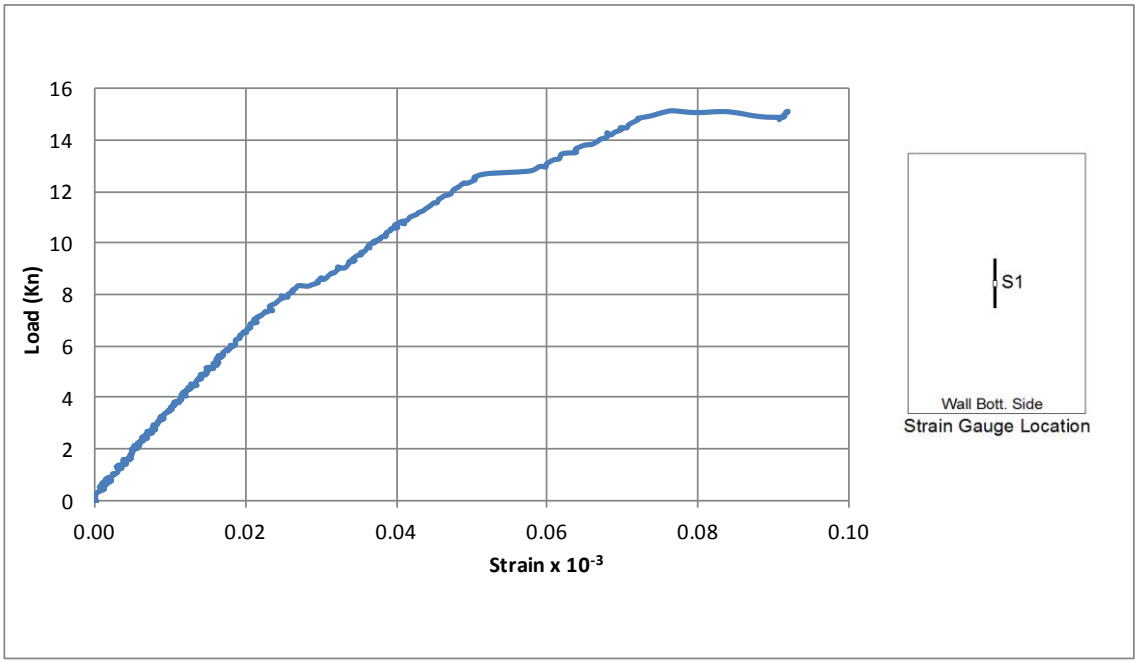

5.5a) Load-strain relationship at strain gauge S1

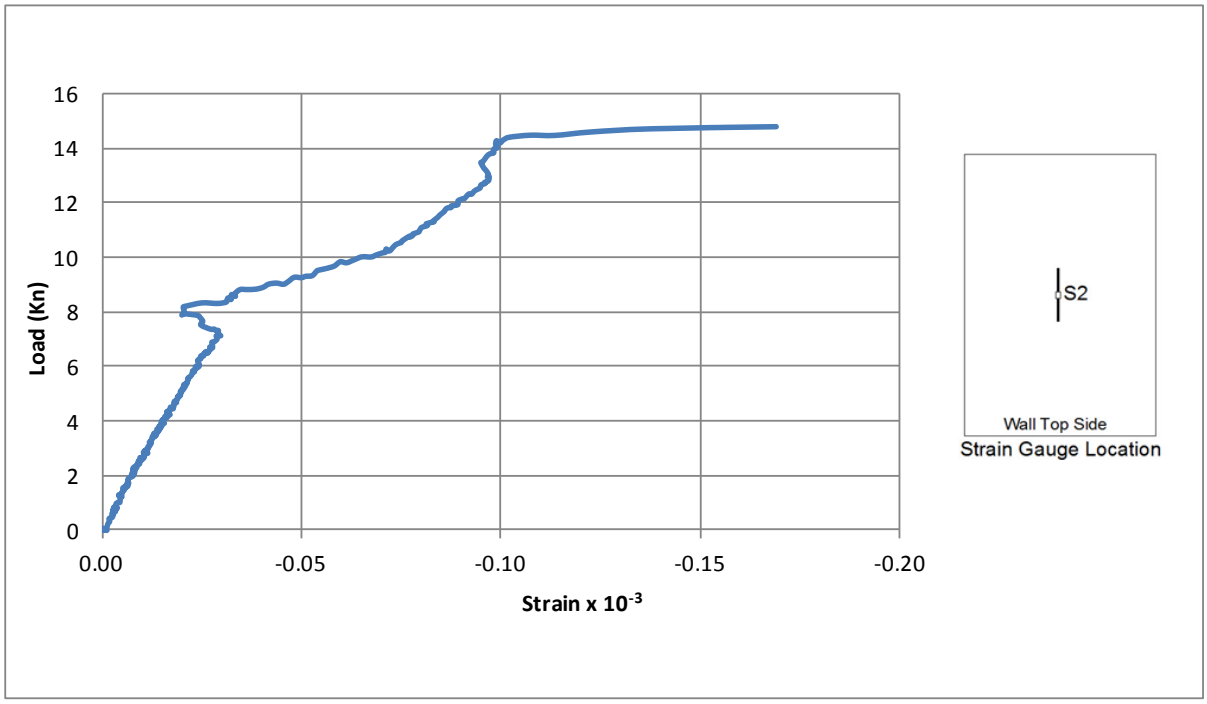

5.5b) Load-strain relationship at strain gauge S2

Figure 5.5: Load-strain relationships for Specimen B5

5.2.1 Failure Modes

Figures 5.6 – 5.10 show the failure of all designation. Failure for all specimens occurred after the load increased up to the ultimate stress of the reinforcement steel mesh. The load-deflection relationship was at first almost linear then it became nonlinear specially after reaching the yielding of the steel mesh and the deformation was observed. The initial stiffness of the test specimens, as indicated by the slope of the linear part of the curve, varied with the properties of the type and distribution of shear connectors.

The average failure load for all designations ranged between 13 kN and 18.8 kN. The crack distributions and patterns were similar to a large extent for all specimens as shown in the next section.

5.2.2 Cracking Pattern

For all designations, vertical crack started to develop from the bottom of the specimens at the ferrocement layer and near the center of the span. Rapidly, the flexure cracks started to propagate vertically towards the top surface at the upper ferrocement layer as the load increased. When the applied load reached the ultimate load, the specimen separated into two parts.

This pattern of the failure could be attributed to the properties of welded steel mesh, which used to reinforce the top layer and the bottom layer of the specimens, and the thickness of the ferrocement layers. The difference between the designations in the cracking pattern was insignificant. However, the average failure load in the different designations was variant because of type and distribution of the shear connectors as shown in this chapter.

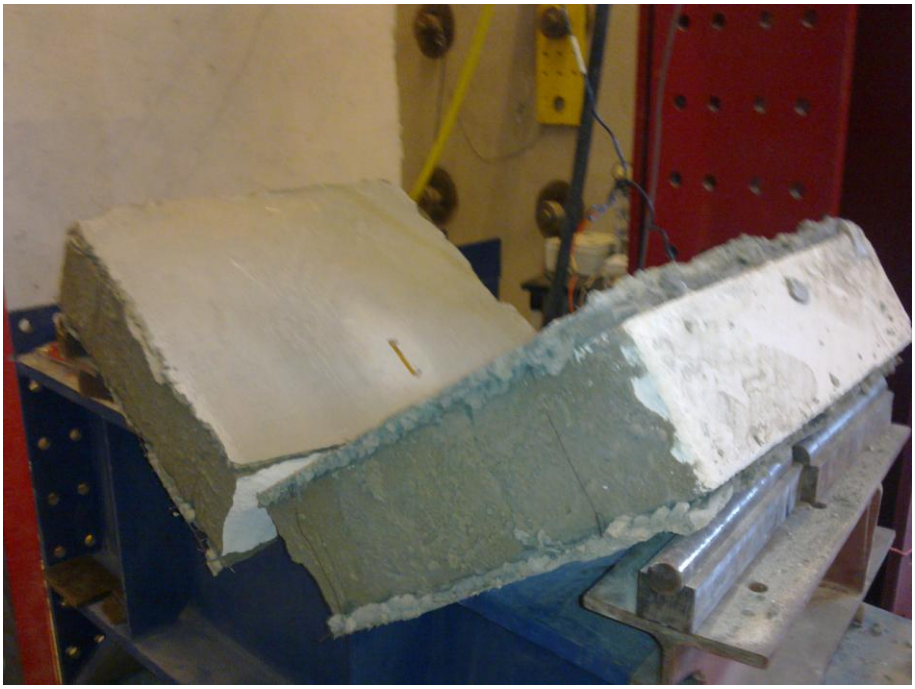

Figure 5.6: Typical failure pattern of specimen B1

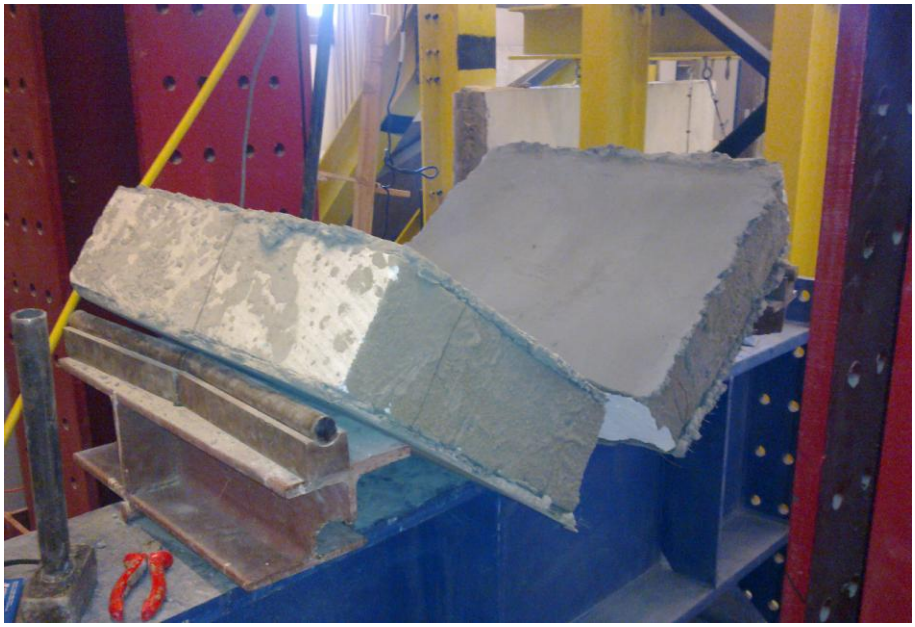

5.7a) Typical failure pattern

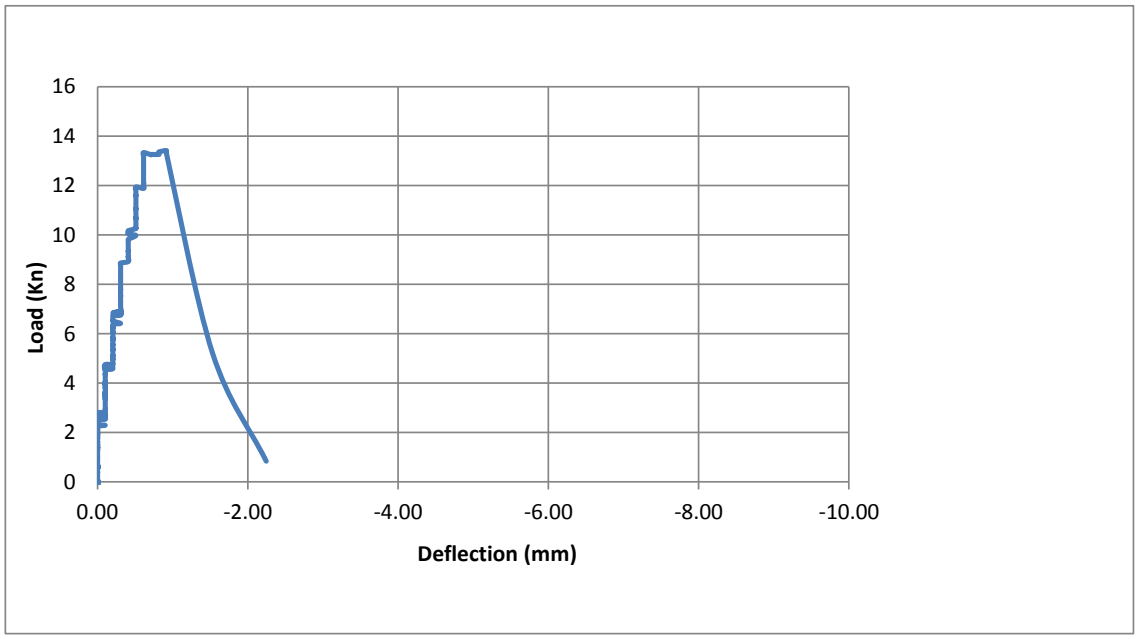

5.7b) Load-deflection relationship

Figure 5.7: Failure of specimen B2

5.8a) Typical failure pattern

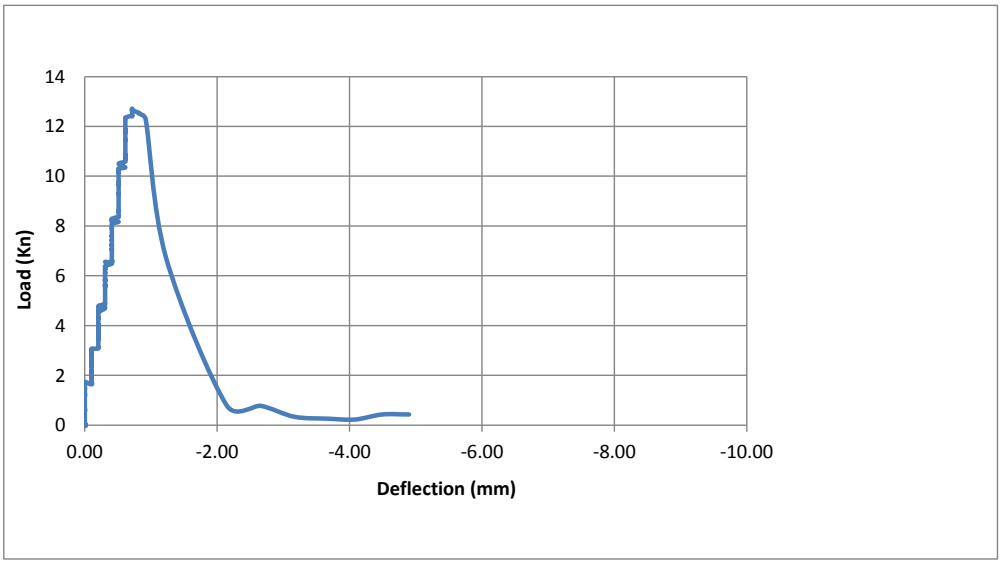

5.8b) Load-deflection relationship

Figure 5.8: Failure of specimen B3

5.9a) Typical failure pattern

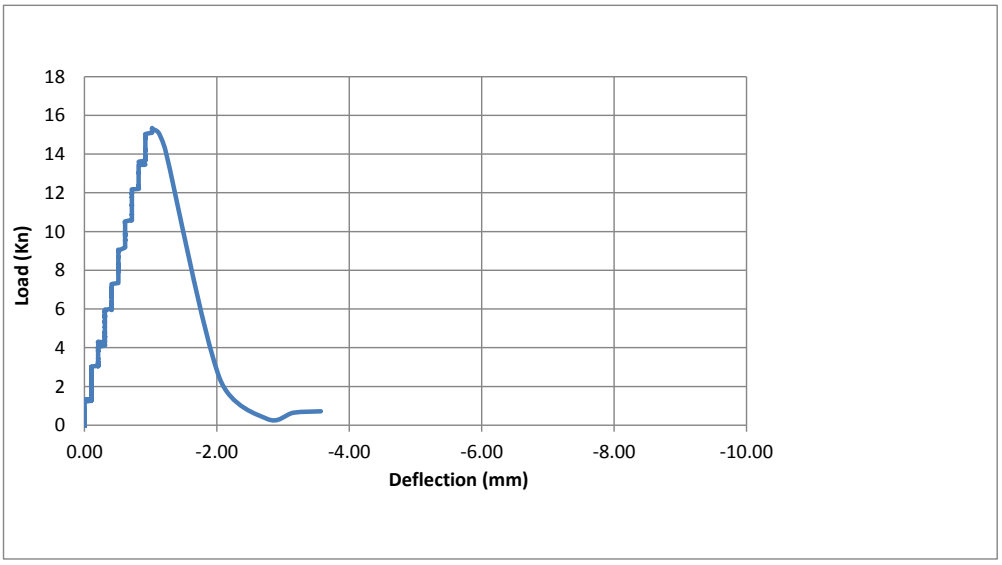

5.9b) Load-deflection relationship

Figure 5.9: Failure of specimen B4

5.10a) Typical failure pattern

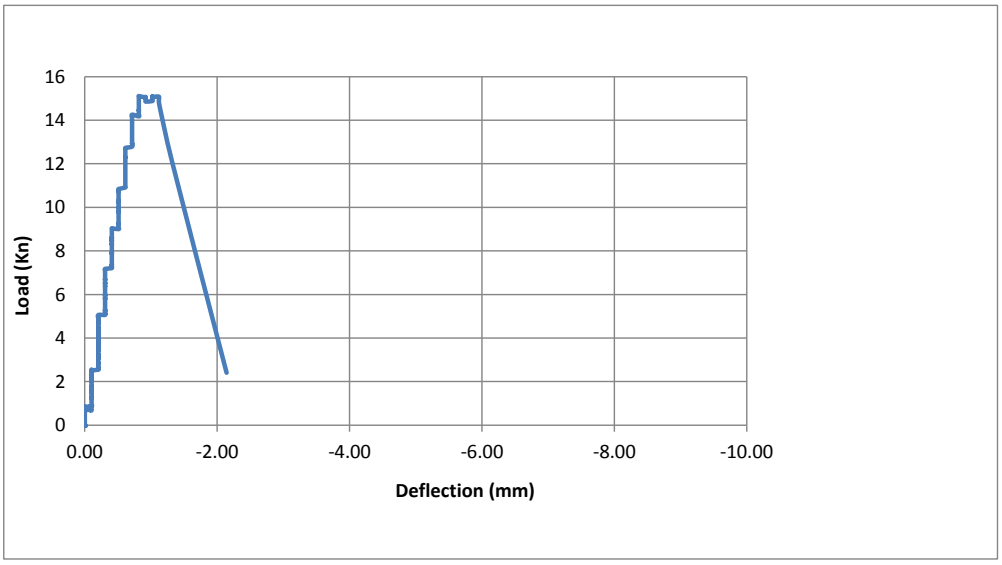

5.10b) Load-deflection relationship

Figure 5.10: Failure of specimen B5

5.3 Parametric Study - Effect of the Type and the Distribution of Shear Connectors

The effect of the type and the distribution of shear connectors could be studied by comparing the results of designation (150-FC-Nails) with those of designation (150-FC- Cross) and with those of designation (150-FC-WM). Using different shear connectors with different distribution resulted in small variance results in the ultimate load as shown in Table 5.1 and Figure 5.11. In case of using WWM as shear connectors instead of cross steel shear connectors with same distribution resulted in slightly increase percentage of ultimate load 117% for designation (150-FC-WM) and (150-FC- Cross). This increase could be attributed to the better bonding between the ferrocement layer and the core brick, which was provided by the WWM shear connector. In case of using nails as shear connectors instead of WWM shear connectors with different distribution resulted in slightly increase the ultimate load with percentage of 123% for designation (150-FC-nails) and (150-FC- WM). Figure 5.12 shows the Load-deflection curves of the specimens B2 and B4.

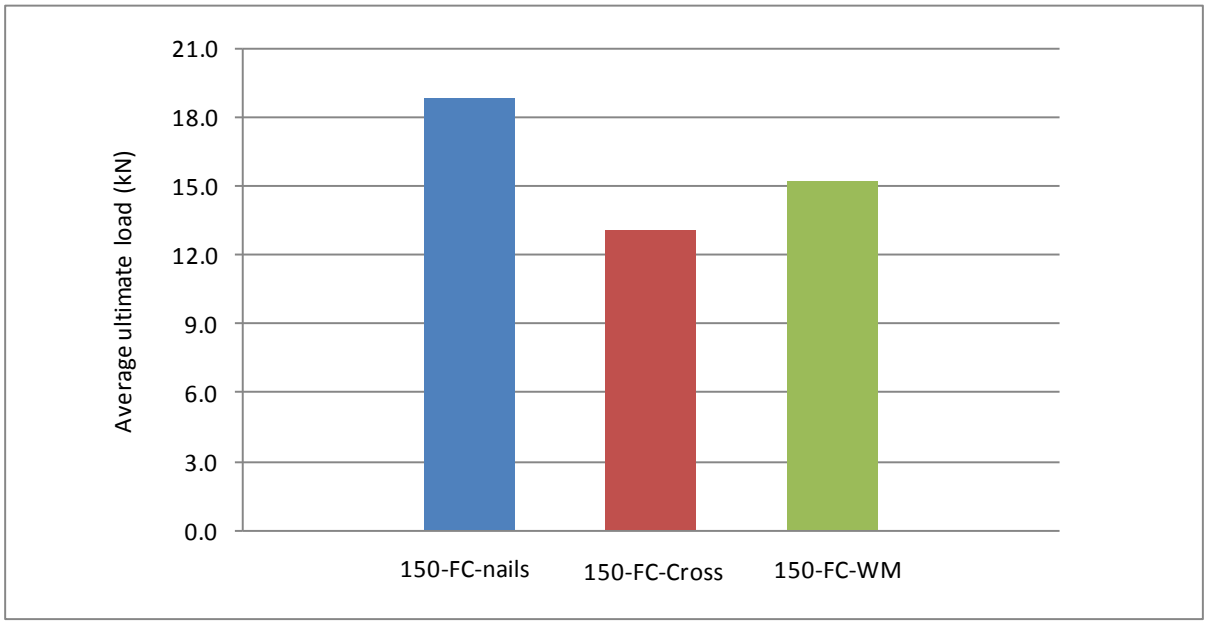

Figure 5.11: Average ultimate load for different designations with varying in shear connectors

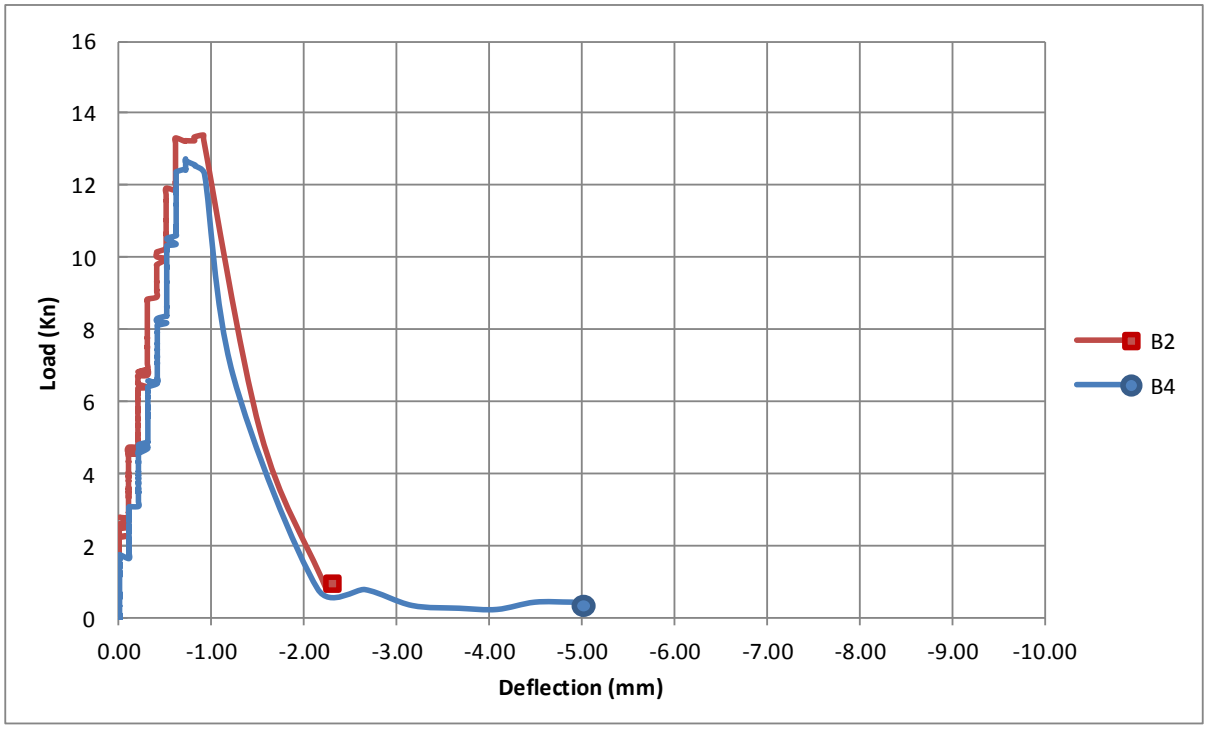

Figure 5.12: Comparison between specimens from designation (150-FC-Cross) and (150-FC-WM)

5.4 Theoretical Calculation of the Ultimate Load

The mode of failure and the ultimate load can be determined theoretically by calculating the shear failure and the bending failure. The ultimate load failure is the smallest values from the bending and the shear failure. In case of bending failure, the analysis of ferrocement slab section has been done by applying the equilibrium of forces and strain compatibility. El-Hlalfawy developed a theoretical model to calculate the ultimate moment, which applied on ferrocement slab (El-Hlalfawy, 2003). The internal forces and the strain distribution with the reinforcement in the ferrocement slab are shown in Figure 5.13. According to the Egyptian Code (Egyptian Code for Design and Construction of Concrete Structures, 2001), the compressive stress is represented by stress block with distance "a", which could be calculated by utilizing the equilibrium forces as follow:

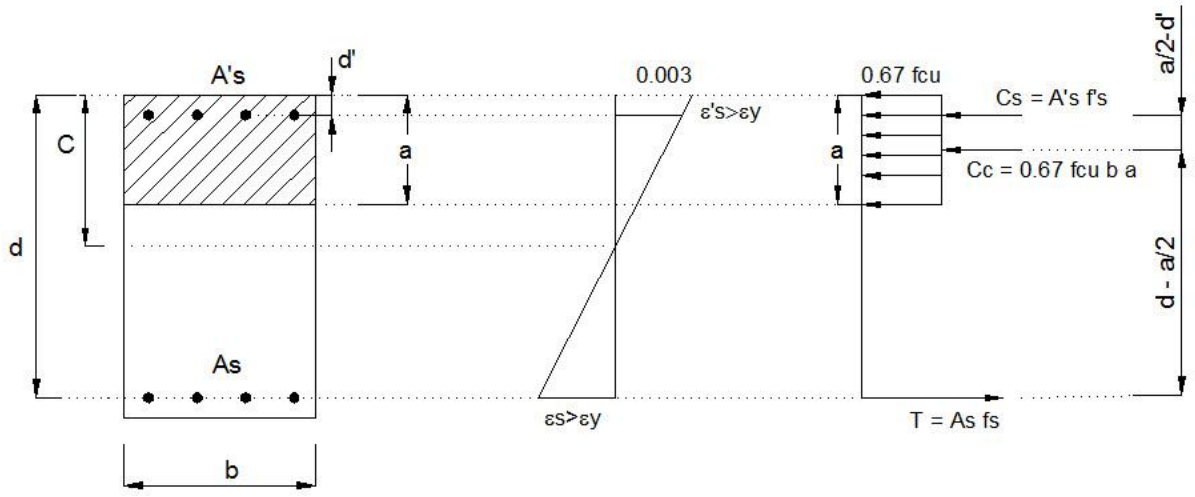

Figure 5.13: Stress and strain distribution of a section

Compression force = Tension force (5.1)

$$C_c + C_s = T \quad (5.2)$$

$$0.67 \times f_{cu} \times b \times a + A'_s \times f_s^{'} = A_s \times f_s \quad (5.3)$$

$$\varepsilon_s = 0.003 \frac{c}{d-c} \quad (5.4)$$

$$f_s = E_s \times \varepsilon_s = 600 \frac{c}{d-c} \quad (5.5)$$

The stress of the compression steel shall be checked by applying the compression steel as follows:

$$\varepsilon'_s = 0.003 \frac{c-d'}{c} \quad (5.6)$$

$$f'_s = E_s \times \varepsilon'_s = 600 \frac{c-d'}{c} \quad (5.7)$$

By applying the previous equations, the location of the neutral axis could be obtained by using the Micorsoft EXCEL sheet program until the equilibrium equation satisfied. By taking the moment of forces around the concrete force the ultimate moment capacity of the section could be determined as follows:

$$M_u = A_s \times f_s (d - \frac{a}{2}) + A'_s \times f_s^{'} (\frac{a}{2} - d') \quad (5.8)$$

By applying Equation 5.8, the ultimate load for bending failure could be determined as follows:

$$M_u = \frac{P_u \times L}{4} \quad (5.9)$$

$$P_u = \frac{4}{L} \times \left[(A_s \times f_s (d - \frac{a}{2}) + A'_s \times f_s^{'} (\frac{a}{2} - d') \right] \quad (5.10)$$

Where:

a = depth of the compression stress block, mm

b = width of the specimen, mm

d = the effective depth of the panel, mm

C = neutral axis depth from the top of the specimen, mm

A_s = area of the steel bars in bottom steel mesh, mm^2

A'_s = area of the steel bars in top steel mesh, mm^2

f_{cu} = the specified characteristic compressive strength of the mortar, N/mm^2

f_s = stress of the steel mesh, N/mm^2

E_s = modulus of elasticity of the steel

ε_s = strain-hardening modulus of the steel

$L_{effective}$ = the effective span of the test specimen, mm

In case of shear failure, the ultimate shear strength Q_u and the ultimate load P_u could be determined according to the Egyptian Code (Egyptian Code for Design and Construction of Concrete Structures, 2001) by applying the following equation:

$$Q_u = \beta \times b \times d \times 0.16\sqrt{f_{cu}} \quad (5.11)$$

$$P_u = 2\ Q_u = 2 \times \beta \times b \times d \times 0.16\sqrt{f_{cu}} \quad (5.12)$$

Where:

β = reduction factor is about 50% for representing the contribution of the loss aggregate in the AAC blocks compared to the ferrocement mortar matrix.

The theoretical ultimate load of each designation was calculated based on its dimensions and its material properties of the AAC brick and the ferrocement according to the Equations 5.10 and 5.12. The theoretical and the experimental results are shown in Table 5.2. The comparison between the experimental and the theoretical in the table shows that the Equations 5.8 and 5.10 reasonably calculates the ultimate load for all designations.

Table 5.2: Comparison between experimental and theoretical ultimate load results.

Specimen No.	Designation	Type of shear connectors	Experimental average ultimate load (kN)	Theoretical average ultimate load (kN)
B1	150-FC-Nails	Nails	18.80	14.30
B2	150-FC-Cross	Steel cross bracing	13.06	14.30
B3	150-FC-Cross	Steel cross bracing		
B4	150-FC-WM	Welded wire mesh	15.23	14.30
B5	150-FC-WM	Welded wire mesh		